



Advanced techniques for estimation of the tensile fracture toughness of adhesive joints

R.D.S.G. Campilho

Departamento de Engenharia Mecânica, Instituto Superior de Engenharia do Porto, Instituto Politécnico do Porto, Rua Dr. António Bernardino de Almeida, 431, 4200-072 Porto, Portugal
raulcampilho@gmail.com

M.D. Banea, L.F.M. da Silva

Departamento de Engenharia Mecânica, Faculdade de Engenharia da Universidade do Porto, Rua Dr. Roberto Frias, s/n, 4200-465 Porto, Portugal

ABSTRACT. Adhesive bonding has become more efficient in the last few decades due to the adhesives developments, granting higher strength and ductility. As a result, adhesives are being increasingly used in industries such as the automotive, aerospace and construction. Thus, it is highly important to predict the strength of bonded joints to assess the feasibility of joining during the fabrication process of components (e.g. due to complex geometries) or for repairing purposes. When using the Finite Element Method with advanced propagation laws, the tensile (G_n^c) and shear (G_s^c) fracture toughness of adhesive joints must be determined with accuracy. Several conventional methods to obtain G_n^c and G_s^c exist in the literature, mainly based on Linear Elastic Fracture Mechanics (LEFM). The J -integral technique is accurate to measure these parameters for adhesives with high ductility. In this work, the J -integral is used to obtain G_n^c by the Double-Cantilever Beam (DCB) test. An optical measurement method is developed for the evaluation of the crack tip opening and adherends rotation at the crack tip during the test, supported by a Matlab® sub-routine for the automated extraction of these quantities. As output of this work, an optical method that allows an easier and quicker extraction of the parameters to obtain G_n^c than the available methods is proposed (by the J -integral technique) and some results are presented regarding joints with different geometry and adherend material.

KEYWORDS. Fibres; Fracture toughness; Damage mechanics; Joining.

INTRODUCTION

The developments in adhesives technology made possible the use of adhesive bonding in many fields of engineering, such as automotive and aeronautical [1]. However, stress concentrations exist in bonded joints along the bond length owing to the gradual transfer of load between adherends and also the adherends rotation in the presence of asymmetric loads [2]. A large amount of works addresses the critical factors affecting the integrity of adhesive joints, such as the parent structure thickness, adhesive thickness, bonding length and geometric modifications that reduce stress concentrations [3-5].

A large number of predictive techniques for bonded joints are currently available, ranging from analytical to numerical, using different criteria to infer the onset of material degradation, damage or even complete failure. Initially, the prediction was performed by theoretical studies as those of Volkersen [6], which had a lot of embedded simplifying assumptions, by



comparing current stresses with the allowable material strengths. Many improvements were then introduced, but these analyses usually suffered from the non-consideration of the material ductility. Fracture mechanics-based methods took the fracture toughness of materials as the leading parameter. These methods included more simple energetic or stress-intensity fracture techniques that required the existence of an initial flaw in the materials [7]. More recent numerical techniques, such as Cohesive Zone Models (CZM), combine stress criteria to account for damage initiation with energetic, e.g. fracture toughness, data to estimate damage propagation [8]. This allows to consider the distinct ductility of adhesives and to gain accuracy in the predictions. All of these fracture toughness-dependent analyses rely on an accurate measurement of G_n^c and G_s^c . CZM in particular can accurately predict damage growth if the fracture laws are correctly estimated [9]. These laws are based on the values of cohesive strength in tension and shear, t_n^0 and t_s^0 , respectively, and also G_n^c and G_s^c . These parameters that cannot be directly related with the material properties measured as bulk, since they account for constraint effects (for adhesive joints, caused by the adherends). The estimation of these fracture parameters is generally accomplished by performing pure tension or shear tests. Regarding G_n^c , the DCB test is the most suitable, due to the test simplicity and accuracy [10]. As described by Suo et al. [11], in the presence of large-scale plasticity, J -integral solutions can also be employed for accurate results, in contrast to LEFM-based solutions. The J -integral is a relatively straight-forward technique, provided that the analytical solution for a given test specimen exists for the determination of G_n^c or G_s^c . The most prominent example is the DCB specimen, for which J -integral solutions are available. It is also possible to estimate the tensile CZM law.

A few methods are available to estimate the cohesive parameters and the respective laws: the property identification and inverse methods consist on assuming a simplified shape (bilinear or trilinear) for the fracture laws and defining the respective parameters by standardized procedures, while the direct method estimates the precise law shape by computing it based on fracture characterization data [12]. This is accomplished by the differentiation of the strain energy release rate in tension (G_n) or shear (G_s) with respect to the relative opening (δ_n for tension or δ_s for shear). A few works addressed the J -integral method. Carlberger and Stigh [13] computed the CZM laws of adhesive layers in tension and shear using the DCB and End-Notched Flexure (ENF) tests, respectively, considering $0.1 \leq t_A \leq 1.6$ mm (t_A is the adhesive thickness). The J -integral methodology and the direct method were used for measurement. The rotation of the adherends was measured by an incremental shaft encoder and the crack tip opening by two Linear Variable Differential Transducers (LVDT). The aforementioned techniques were considered accurate and enabled extracting the parameters with little noise during the full range of the tests. Nonetheless, added difficulties were found because of the complicated test setup. The value of G_n^c revealed a monotonic increase from $t_A=0.1$ to 1.0 mm. Above this value, a slight reduction was found. Under shear, the dependence of G_s^c with t_A is not so significant, but an identical increasing trend is clear under $t_A=0.2$ mm. In both cases, the observed behavior was explained in light of the increasing plastic zone size with the corresponding increase of t_A . Ji et al. [14] studied by the J -integral the influence of t_A in DCB joints on t_n^0 and G_n^c for a brittle epoxy adhesive. G_n^c was measured by a direct technique. For the measurement of the adherends rotation, two digital inclinometers with a 0.01° precision were attached at the free end of each adherend. The normal displacement at the crack tip was measured by a charge-coupled device (CCD) camera. Regarding the test setup, a step forward in terms of procedure was achieved by replacing the opening measurement system by a non-contact system. Regarding the influence of t_A on G_n^c , an increasing trend was found from $0.09 \leq t_A \leq 1.0$ mm, which was related to increasing plastic dissipations with the increase of t_A .

This work evaluates G_n^c of adhesive joints for different conditions: adhesive bonding for adhesive joints with natural fibre composite as adherends, adhesive bonding between aluminium adherends to study the effect of the adherends thickness (b) on G_n^c , and finally adhesive bonding between aluminium adherends considering varying values of t_A . The J -integral is selected to measure G_n^c to account for the plasticity effects, together with the direct method to define the cohesive laws. An optical measurement method is used for the evaluation of crack tip opening and adherends rotation at the crack tip, supported by a Matlab® routine for the automated extraction of these parameters. This technique provides a step forward in the available methods to extract the adherends rotation and crack opening at the crack tip, enabling a much easier test setup, without compromising the accuracy of the results. The data analysis is also automated to ease the data reduction process.

EXPERIMENTAL WORK

Characterization of the materials

Three joint configurations were tested in this work, presented in Tab. 1, considering the DCB test geometry. For configuration 1, typical properties of jute are as follows: density of 1.3-1.4 g/cm³, elongation at failure (ϵ_f) of 1.5-1.8%, tensile strength (σ_f) of 400-800 MPa and Young's modulus (E) of 15-30 GPa [15, 16]. Epoxy was chosen



for the matrix material on account of the good mechanical (strength and stiffness) and toughness properties, and also because of the superior wetting characteristics on natural fibres [17]. The epoxy resin type SR 1500 and SD 2505 hardener from Sicomin Epoxy Systems were used. The matrix properties, as specified by the manufacturer, are as follows: $E=3.1$ GPa, $\sigma_f=74$ MPa, strain at maximum load $\varepsilon_m=4.4\%$ and $\varepsilon_f=6.0\%$. The jute-epoxy composite was composed by 30% of jute fabric (by weight) and gave the following properties in tensile testing: $E=5.7$ GPa and $\sigma_f=124.3$ MPa. For configurations 2 and 3, the aluminium adherends were cut from a high strength aluminium alloy sheet (AA6082 T651).

Configuration	Adherends	Adhesive
1	Jute-epoxy composite	SikaForce® 7888
2	Aluminium	SikaForce® 7888
3	Aluminium	SikaForce® 7752-L60

Table 1: Configurations tested to measure G_n^c .

This material was characterized in bulk tension in previous works by the authors [18] using dogbone specimens and the following mechanical properties were obtained: $E=70.07\pm 0.83$ GPa, tensile yield stress (σ_y) of 261.67 ± 7.65 MPa, ultimate tensile stress (σ_f) of 324 ± 0.16 MPa and elongation (ε_f) of $21.70\pm 4.24\%$. Configurations 1 and 2 used the polyurethane adhesive SikaForce® 7888, which was characterized in the work of Neto et al. [19] by bulk tensile tests for the determination of E , σ_f and ε_f , and DCB and ENF tests to define the values of G_n^c and G_s^c , respectively. The bulk characterization was performed as specified in the EN ISO 527-2 standard [20]. The obtained results gave $E=1.89\pm 0.81$ GPa, $\sigma_f=28.60\pm 2.0$ MPa, $\varepsilon_f=43.0\pm 0.6\%$, $G_n^c=0.7023\pm 0.1233$ N/mm and $G_s^c=8.721\pm 0.792$ N/mm. Configuration 3 used a novel polyurethane structural adhesive, SikaForce® 7752-L60. This is a two-part adhesive, and it consists of a filled Polyol based resin and an Isocyanate based hardener. It is characterized by a room temperature cure, high impact resistance and flexibility at low temperatures, having a tensile strength of approximately 10 MPa and tensile failure strain of 25% (manufacturer's values).

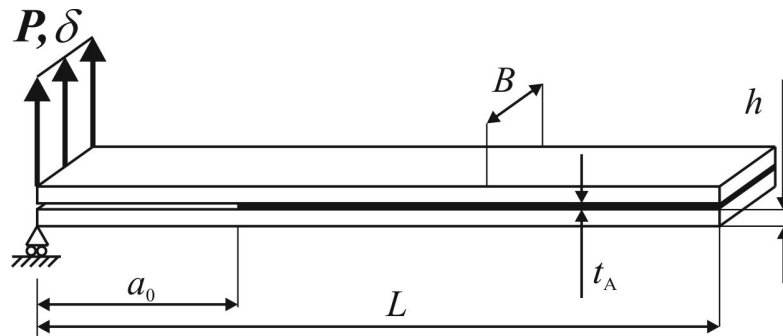


Figure 1: Geometry and characteristic dimensions of the DCB specimens.

Configuration	L (mm)	a_0 (mm)	b (mm)	B (mm)	t_A (mm)
1	160	50	5	15	1
2	160	40	1, 2, 3 and 4	25	1
3	160	55	3	25	0.1, 0.2, 0.5, 1.0 and 2.0

Table 2: Dimensions of the three joint configurations.

Joint geometries

The geometry of the DCB specimens is shown in Fig. 1. The characteristic dimensions are the total length (L), initial crack length (a_0), b , width (B) and t_A . The chosen values for each joint configuration are presented in Tab. 2. Some dimensions differ between configurations, but these do not affect the G_n^c measurement. The joints for configuration 1 considered jute-epoxy composites as adherends, consisting of 8 stacked weave plies with a fibre volume fraction of approximately

30%. The plates were fabricated by hand lay-up and cured at room temperature in a vacuum bag. For the three joint configurations, for a uniform value of t_A , calibrated spacers were inserted between the adherends. These spacers were inserted at both bonding edges between the adherends to control the value of t_A . For the calibrated spacer at the crack tip, 3 plies were stacked and glued together, composed of a 0.1 mm thick razor blade between steel spacers to achieve the desired value of thickness, to create a pre-crack. For all specimens, stainless steel piano hinges were glued to both faces of the specimens at the cracked edge with a ductile adhesive, to provide a loading means in the testing machine grips. Also, a metric scale was glued with cyanoacrylate in both adherends to allow measurement of the crack length (a) and of the input data for the extraction of the J -integral. Six specimens of each configuration were tested at room temperature ($\approx 20^\circ\text{C}$), relative humidity of $\approx 40\%$ and 2 mm/min in an electro-mechanical testing machine (Shimadzu AG-X 100) with a load cell of 100 kN. Data recording was carried out at 5 Hz for the load (P) and testing machine grips displacement (δ), registered during the test as a function of the time elapsed since its initiation. Pictures were recorded during the specimens testing with 5 s intervals using a 15 MPixel digital camera with no zoom and fixed focal distance to approximately 100 mm.

J-INTEGRAL TECHNIQUE TO MEASURE G_n^c

In the proposed method, the CZM law is measured by the direct method. Under this scope, the path-independence of the J -integral can be used to extract relations between the specimen loads and the cohesive law of the crack path [21]. Based on the fundamental expression for J defined by Rice [22], it is possible to derive an expression for the value of G_n applied to the DCB specimen from the concept of energetic force and also the beam theory for this particular geometry, as follows [23]:

$$G_n = 12 \frac{(P_u a)^2}{E b^3} + P_u \theta_o \quad \text{or} \quad G_n = P_u \theta_p \quad (1)$$

where P_u represents the applied load per unit width at the adherends edges, θ_o the relative rotation of the adherends at the crack tip and θ_p the relative rotation of the adherends at the loading line (Fig. 2).

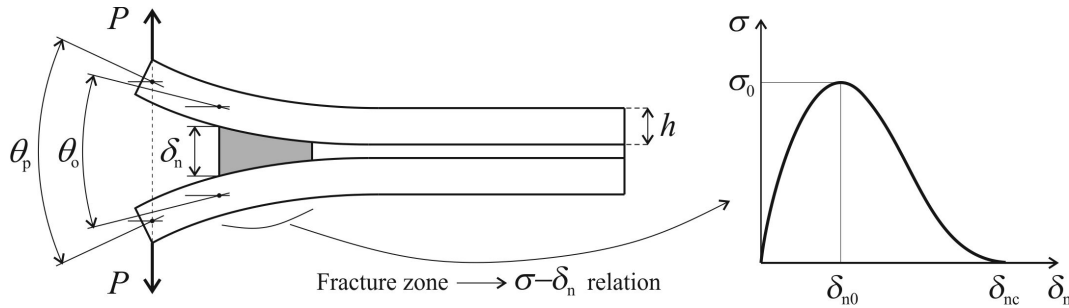


Figure 2: DCB specimen under loading, with description of the analysis parameters.

In this work, the first expression of (1) is considered, using θ_o instead of θ_p , due to a simpler extraction of the parameter by the optical method. The J -integral can be calculated along an arbitrary path encircling the start of the adhesive layer, giving [21]:

$$G_n = \int_0^{\delta_{nc}} t_n(\delta_n) d\delta_n \quad (2)$$

where δ_{nc} is the end-opening at failure of the cohesive law (measured at the initial crack tip) and t_n is the current normal traction. G_n^c can be considered the value of G_n at the beginning of crack growth. Thus, G_n^c is given by the steady-state value of G_n , at a δ_n value of δ_{nc} [13]. The $t_n(\delta_n)$ curve can be easily obtained by differentiation of Eq. (1) with respect to δ_n

$$t_n(\delta_n) = \frac{\partial G_n}{\partial \delta_n} \quad (3)$$

As a result, the procedure of an experiment is to measure the history of P , a , δ_n and θ_0 . The cohesive law in tension can then be estimated by plotting G_n in Eq. (1) as a function of δ_n , polynomial fitting of the obtained curve and differentiation [21].

Optical method for the parameter measurement

For calculating δ_n and θ_0 for a given image, the optical method requires the identification of eight points (Fig. 3): two points (p_1, p_2) for measuring the current t_A value at the crack tip (t_{A}^{CT}) during loading in image units (pixels), two points (p_3, p_4) identifying a line segment in the image for which the length (d) is known in real world units (mm), two points (p_5, p_6) on the top specimen and two points (p_7, p_8) on the bottom specimen.

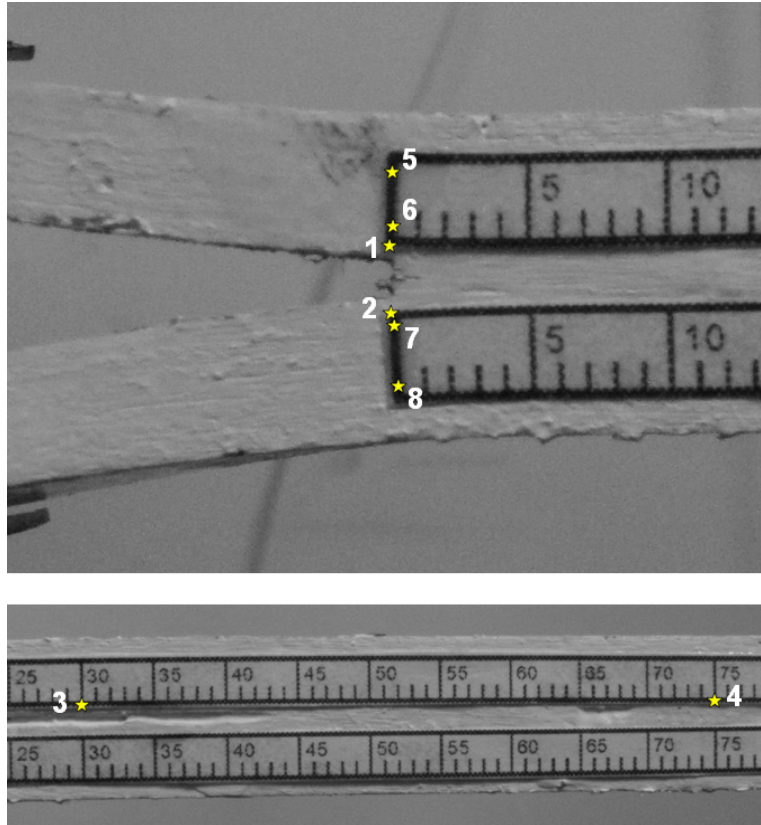


Figure 3: Points taken by the optical method for measuring θ_0 and G_n^c .

Points Identification

All eight points are manually identified in the first picture of a trial using an in-house software tool. The identification of the points is aided by the ruler attached to the specimens. Using the location of the points in the first picture, the points of the following pictures are automatically identified using a computer algorithm implemented in Matlab[®]. Basically, for each point p_i , a rectangular region centred in p_i is extracted from the first image forming a template (t). This template describes the image pattern that surrounds the point and is used for locating the point in the next image. This is done by finding the position (u, v) in the next image (I) that has the highest normalized cross-correlation with the template. The normalized cross-correlation is a measure of similarity between two grayscale images that is invariant to linear changes in illumination and that quantifies the correlation between the grayscale levels of two images/regions. The normalized cross-correlation (γ) of template t with image I at the position (u, v) of image I is defined as:

$$\gamma(u, v) = \frac{\sum_{x,y} [f(x, y) - \bar{f}_{u,v}] \cdot [t(x-u, y-v) - \bar{t}]}{\left\{ \sum_{x,y} [f(x, y) - \bar{f}_{u,v}]^2 \cdot \sum_{x,y} [t(x-u, y-v) - \bar{t}]^2 \right\}^{0.5}} \quad (4)$$

where f is the region of the image I with the same size as t centred in the position (u,v) . Calculating γ for all the pixels of I results in a matrix, where the maximum absolute value yields the location of the region in I that has the highest correlation with t and, thus, the most likely location of p_i in the next image. This is done for every one of the eight points identified in the first image. After successfully identifying all the points of the second image, new templates are computed from the second image to search for the eight points in the third image, and so on until processing all the images.

Computation of δ_n

The value of t_A^{CT} in real world units (mm) is calculated as follows

$$t_A^{CT} = d \frac{|p_1 - p_2|}{|p_3 - p_4|} \quad (5)$$

For all trials, a region of length $d=45$ mm was used (Fig. 3). The pixel size was on average 0.024 mm and, thus, the estimated maximum error of the image acquisition process is ± 0.012 mm. Finally, δ_n can be defined as

$$\delta_n = t_A^{CT} - t_A \quad (6)$$

where t_A is the theoretical design value of 1 mm. Since t_A can show small variations due to the fabrication process, an adjustment to δ_n is also applied to make $\delta_n=0$ at the beginning of the test. Fig. 4 gives an example of the evolution of δ_n for a selected test specimen of configuration 2 (with $h=4$ mm). Shown in the graphic are the raw curve, the 6th degree fitting curve and the corrected polynomial and final curve, adjusted to make δ_n (testing time=0)=0. This polynomial adjustment is required to smooth the raw data and remove experimental measurement scatter, but also to cancel any eventual misalignment between glued scales in both adherends.

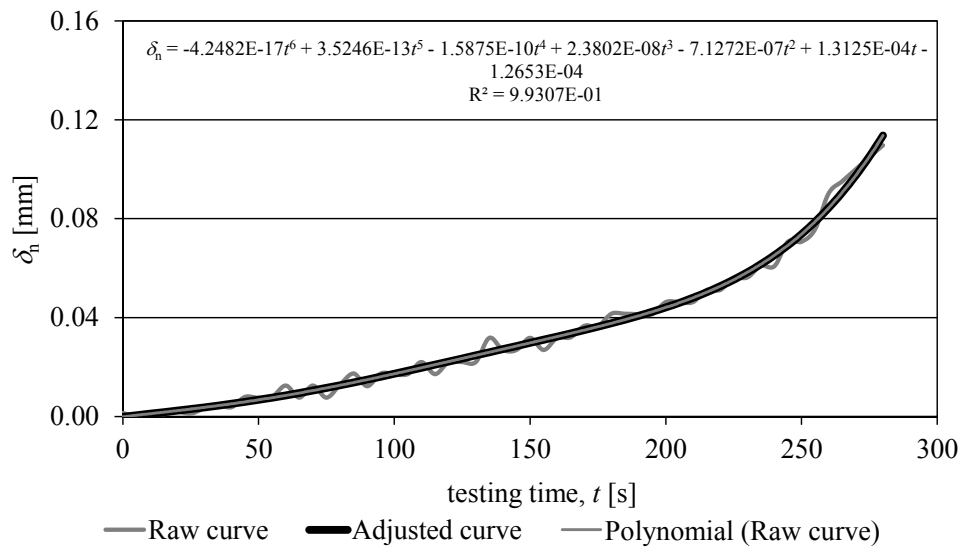


Figure 4: Evolution of δ_n for one test specimen: raw curve obtained from the optical method, polynomial fitting curve and corrected polynomial curve.

Computation of θ_0

θ_0 is calculated as the angle between lines l_1 and l_2 (Fig. 5). These lines could be directly calculated from points (p_5, p_6) and (p_7, p_8) respectively. However, for increasing robustness to small fluctuations of the point detection process, an image processing algorithm was used to extract the midline of the edge of the ruler that contains the pair of points in hand. In particular, a Difference of Gaussian filters was applied for enhancing the edges of the ruler, resulting in an image where pixels belonging to edges have high intensity values, while the remaining ones have low intensity (Fig. 5).

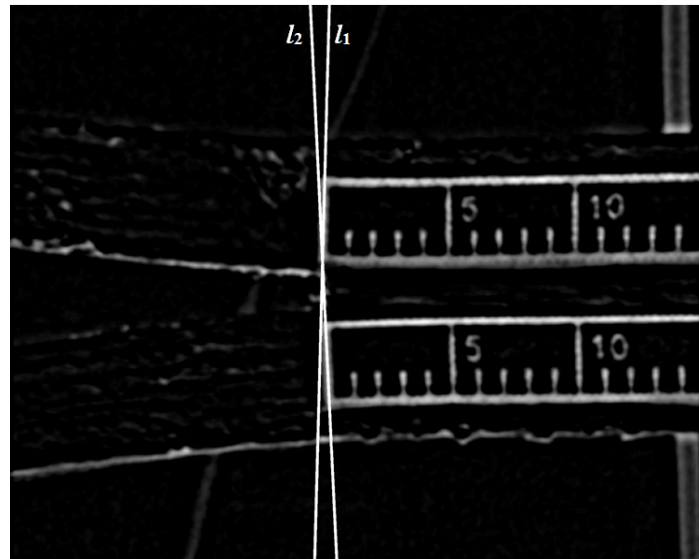


Figure 5: Image after applying the Difference of Gaussian filters and the extracted lines (l_1 and l_2) that are used for measuring θ .

Then, for the rows of the image between p_5 and p_6 , the midpoint of the edge at each row is computed. The midpoint is first extracted for the row of p_5 by (1) collecting all the pixels to the left and to the right of p_5 that can be reached from p_5 without dropping the pixel intensity below a given threshold (10% for all experiments), and (2) by averaging the position of all the collected pixels weighted by the pixels intensity value (so that pixels with higher intensities, i.e. pixels belonging to the edge, have a higher impact in the row's midpoint calculation). This makes the process robust to blur in the images and to the point identification process because points p_5 and p_6 do not need to be identified exactly in the midline of the edge. This process is repeated for all the following rows until reaching p_6 , resulting in one point per row of the image between p_5 and p_6 that define the midline of the edge of the ruler. Since these points are not necessarily collinear, a linear regression is used for obtaining l_1 . The same process is repeated with points (p_7, p_8) for obtaining l_2 and, finally, θ_0 may be calculated as the angle between the two lines

$$\theta_0 = \arccos\left(\frac{\vec{v}_1 \cdot \vec{v}_2}{|\vec{v}_1| |\vec{v}_2|}\right) \quad (7)$$

where \vec{v}_1 and \vec{v}_2 are the direction vectors of lines l_1 and l_2 , respectively. Fig. 6 shows the θ_0 -testing time plot for a specimen, more specifically the three curves of Fig. 4. Due to scaling difficulties, the raw curve in the figure is already translated such that $\theta_0(\text{testing time}=0)=0$.

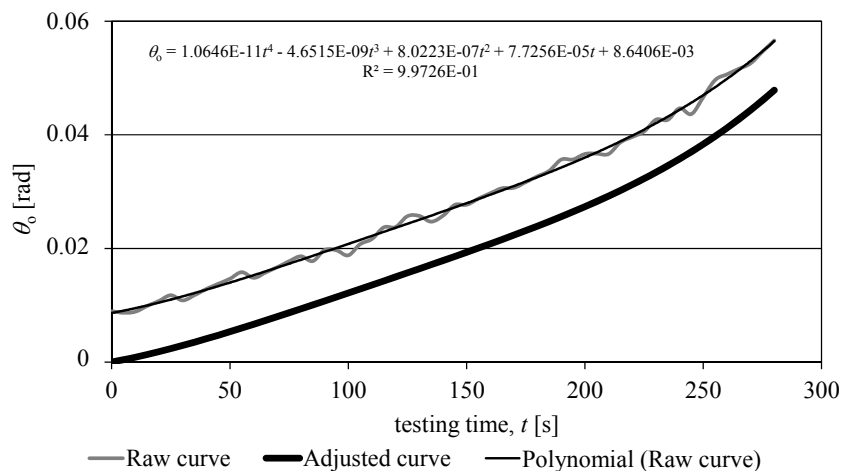


Figure 6: Evolution of θ_0 for one test specimen: raw curve obtained from the optical method, polynomial fitting curve and corrected polynomial curve.



RESULTS

Configuration 1

For the bonded specimens with jute-epoxy adherends, δ_n and θ_0 were defined as specified previously. The values of G_n^c for the bonded joints were defined by plotting the G_n - δ_n curves, considering G_n^c as the steady-state value of G_n in the G_n - δ_n curve [13]. Fig. 7 plots the experimental G_n - δ_n law and the corresponding 6th degree polynomial fitting curve for a given specimen. At the beginning of the test, G_n slowly increases with δ_n , but the growth rate of G_n rapidly increases up to nearly $\delta_n=0.02$ - 0.04 mm, and a steady-state value of G_n is attained at approximately $\delta_n = 0.09$ mm. For this specimen, the measured value of G_n^c is 1.429 N/mm. For the six bonded specimens, the obtained data gave $G_n^c=1.182\pm 0.215$ N/mm. Fig. 8 shows the obtained experimental t_n - δ_n law, showing the ductile characteristics of the adhesive after the peak value of t_n is attained. For this specimen, the following values were found: $t_n^0=20.73$ MPa and $\delta_{nc}=0.0935$ mm. For the complete batch of tested specimens, average values and deviations were as follows: $t_n^0=23.18\pm 3.57$ MPa and $\delta_{nc}=0.0843\pm 0.156$ mm. Proposed triangular and trapezoidal simplified CZM laws are also presented, allowing concluding that for the adhesive SikaForce[®] 7888 a trapezoidal law is particularly suited, since it accounts the best for the adhesive ductility.

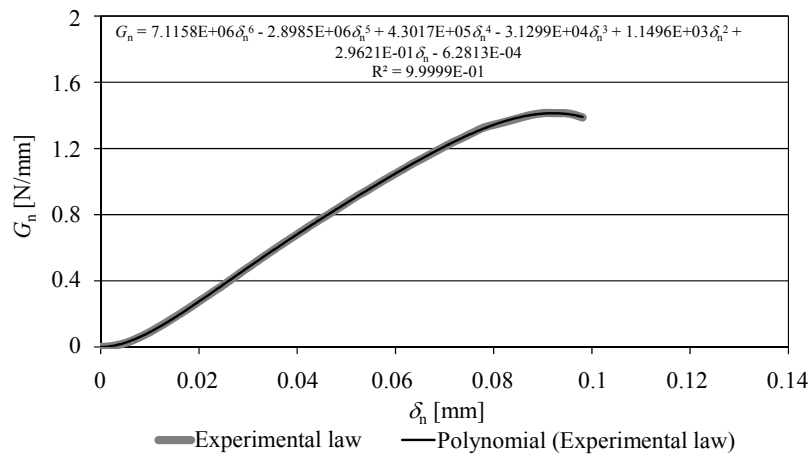


Figure 7: Experimental G_n - δ_n law for one test specimen and polynomial fitting curve (configuration 1).

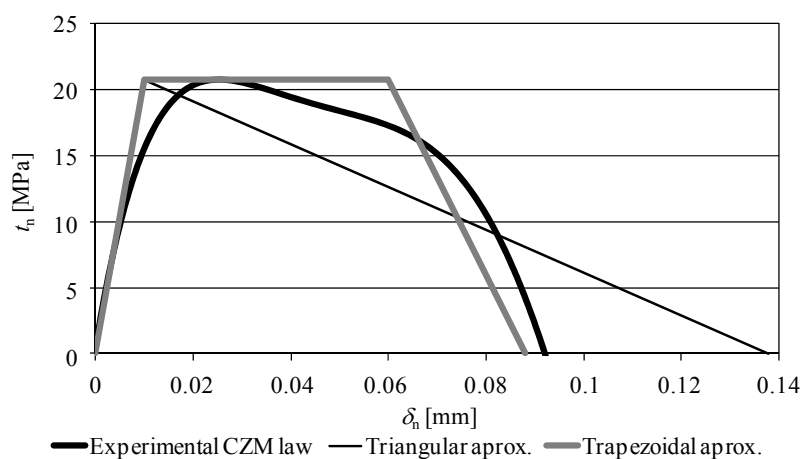


Figure 8: Experimental t_n - δ_n law for one test specimen.

Configuration 2

G_n^c was calculated by Eq. (1). The experimental G_n - δ_n laws were identical in shape to Fig. 7, and an example for $b=3$ mm is presented in Fig. 9. The G_n^c results by applying this procedure for all tested specimens are shown in Fig. 10 as a



function of b . The deviation is somehow large, and whose justification lies on the experimental process to obtain G_n^c , which relies on a number of measured parameters and approximation functions, which are difficult to adjust to the experimental data [24]. While for the specimens with $b=1$ mm, a value of $G_n^c=0.781\pm 0.146$ N/mm was obtained, improvements of 12.6, 37.7 and 40.2% were attained by increasing b up to 4 mm. These results show the stabilization of G_n^c for a given value of b (in this case between $G_n^c=1.075\pm 0.226$ N/mm for $b=3$ mm and $G_n^c=1.095\pm 0.195$ N/mm for $b=4$ mm a stabilization of G_n^c was found).

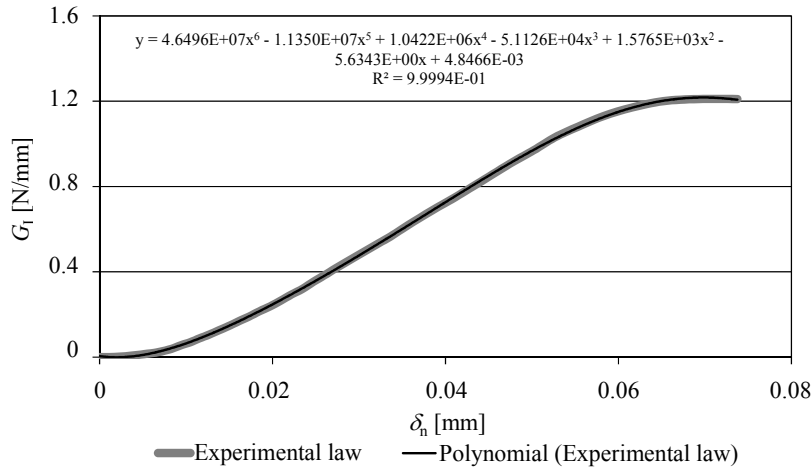


Figure 9: Experimental G_n - δ_n law for one test specimen with $b=3$ mm and polynomial fitting curve (configuration 2).

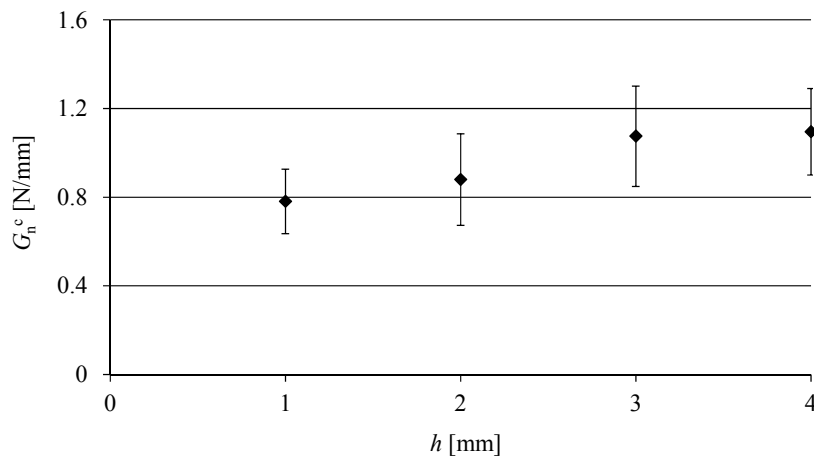


Figure 10: Average values and deviation of G_n^c as a function of b by the J -integral.

This increase of G_n^c is reported in the literature because of the stress field variations ahead of the crack tip being dependent on the joint geometry, which highly influences the shape and size of the damage zone, and the local yield stress as well [25]. As it was discussed in previous works [26], thicker adherends provide an elevation of peel stresses further within the joint, shifting the loading conditions from peeling to cleavage, and giving a larger length for the damage zone. These findings are corroborated in the work of Azari et al. [27], regarding the adherend stiffness influence on the fatigue failure of bonded joints, which proved by Finite Elements that the plastic zone in adhesive joints between steel adherends was consistently higher than identical joints between aluminium adherends during the entire damage uptake process up to crack initiation. Mangalgiro et al. [28] justified this tendency with the plastic zone and stress distributions ahead of the debond tip. Actually, the plastic zone was bigger in length across the adhesive layer with increasing number of composite plies (and thus, increasing b). Also, thicker adherends used a larger amount of the input energy to the specimen to develop a lengthier plastic zone, thus leaving less available energy for damage growth [29]. On account of this, higher values of G_n^c can be expected for joints with higher degrees of restraint (i.e., stiffer or thicker adherends).

Configuration 3

Following the method described in *J-integral technique to measure G_n^c* section, G_n^c was calculated identically to the previous cases, which considered θ_o instead of θ_p to obtain G_n . The aforementioned method was applied to all tested specimens and the G_n^c results for each t_A value and respective deviation are presented in Fig. 11. For the specimens with $t_A=0.1$ mm, the obtained results gave $G_n^c=1.83\pm 0.24$ N/mm. The increase of G_n^c from this point was of 14.5% ($t_A=0.2$ mm), 57.8% ($t_A=0.5$ mm), 105.6% ($t_A=1.0$ mm) and 195.9% ($t_A=2.0$ mm).

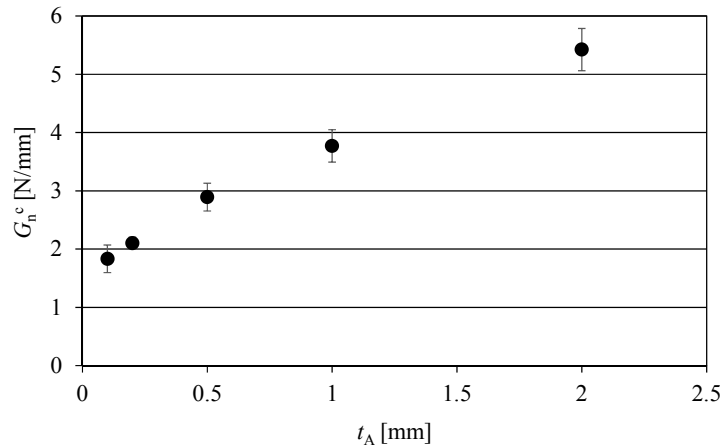


Figure 11: Average values and deviation of G_n^c as a function of t_A by the *J*-integral.

Regarding the available studies (for epoxy adhesives), Yan et al. [30] studied the influence of t_A on the fracture properties (G_n^c) of DCB and Compact Tension (CT) joints with aluminium adherends and a rubber-modified epoxy adhesive. Using a large deformation Finite Element technique and the peak loads measured in the experiments, the critical value of the *J*-integral was calculated for different values of t_A . A G_n^c increase was found up to $t_A=1$ mm and a decrease afterwards. An identical conclusion was found by Khoo and Kim [31] for an epoxy adhesive between $0.2 < t_A < 1.5$ mm, with the maximum G_n^c being found for $t_A=1$ mm. The increasing trend obtained in this work of G_n^c with t_A is linear up to $t_A=2.0$ mm, and this result is consistent with previous studies in this matter, except from a reduction of G_n^c for big values of t_A that is common with less ductile epoxy adhesives. Another exception is the work of Marzi et al. [32], which attained a maximum G_n^c between $t_A=1$ and 2 mm for the polyurethane SikaPower 498TM, a modern crash resistant epoxy adhesive, without a reduction tendency of G_n^c up to $t_A=2$ mm, due to its large ductility. An identical trend to this work regarding the G_n^c - t_A law was found by Banea et al. [33] with the high elongation polyurethane adhesive Sikaforce® 7888, characterized with conventional fracture methods in the range of $0.2 \leq t_A \leq 2$ mm. In both this and the present work, the peak value of G_n^c is attained for a t_A value bigger than 2 mm, but in this range of values the joints are more likely to have fabrication defects, and be more difficult to fabricate, which justifies its limited industrial applicability.

Discussion of results

The proposed technique, applied to the 3 joint configurations, showed that the proposed *J*-integral methodology can be a valuable tool to estimate G_n^c of adhesive joints. Moreover, with the measurement of δ_n , the cohesive law of the adhesive layer can be obtained as well. By analyzing the obtained results between the three tested configurations, a direct analogy cannot be formed between configuration 3 and configurations 1 and 2, because a different adhesive was considered (although both tested adhesives are ductile polyurethanes). In the comparison between configurations 1 and 2, it should be noted that, as depicted in Tab. 2, the value of b varied. This has a significant influence on the plastic zone size and, thus, also on the G_n^c measurements. The measured data for the bonded joint of configuration 1 gave $G_n^c=1.182\pm 0.215$ N/mm ($b=5$ mm), while for configuration 2 and $b=4$ mm the value of $G_n^c=1.095\pm 0.195$ N/mm was obtained. These values agree quite well, although the difference in bending stiffness of the adherends has to be considered: the values of b between these two configuration differ and, additionally, the value of E of the adherends for configuration 2 (aluminium) is much higher than that of configuration 1 (jute-epoxy composite). Since the results of configuration 2 show that, for aluminium adherends, for b values above 3 mm the plastic zone effect ceases to affect the results, the G_n^c measurement theoretically should be identical between configurations 1 and 2. In view of this discussion, the 7.4% different between these two configurations is attributed to experimental scatter and related issues.



CONCLUDING REMARKS

This work dealt with the determination of G_n^c of adhesive joints with different configurations, considering either the adhesive or adherend material. The J -integral was used to measure G_n^c , given the large adhesive plasticity. With this purpose, an optical measurement and data analysis method was built in Matlab® to extract θ_0 to obtain G_n , and δ_n to build the CZM laws. The complete tensile CZM law of the adhesive was derived by the direct method in some cases, on account of the available G_n - δ_n curve that was differentiated to provide the t_n - δ_n (or CZM) law. For configuration 1, an average value of $G_n^c=1.182$ N/mm was obtained for the adhesive Sikaforce® 7888 between jute-epoxy composite adherends. This value can be compared to the average of $G_n^c=1.095$ N/mm estimated in configuration 2 for $b=4$ mm aluminium adherends. These values agree quite well, although it should be considered that both configurations differ in the values of b and E of the adherends. A direct analogy cannot be formed between configuration 3 and configurations 1 and 2, because a different adhesive was considered. As output of this work, G_n^c data was given for the strength prediction of bonded joints for different adhesives and joint conditions. Additionally, a methodology was presented to accurately estimate G_n^c for ductile adhesives, as well as the CZM law, which can be used for strength predictions of bonded structures by CZM modelling.

REFERENCES

- [1] Lee, M.J., Cho, T.M., Kim, W.S., Lee, B.C., Lee, J.J., Determination of cohesive parameters for a mixed mode cohesive zone model, *Int. J. Adhes. Adhes.*, 30 (2010) 322-328.
- [2] Pinto, A.M.G., Magalhães, A.G., Campilho, R.D.S.G., de Moura, M.F.S.F., Baptista, A.P.M., Single-lap joints of similar and dissimilar adherends bonded with an acrylic adhesive, *J. Adhesion*, 85 (2009) 351-376.
- [3] Campilho, R.D.S.G., Pinto, A.M.G., Banea, M.D., Silva, R.F., da Silva, L.F.M., Strength improvement of adhesively-bonded joints using a reverse-bent geometry, *J. Adh. Sci. Technol.*, 25 (2011) 2351-2368.
- [4] Deng, J., Lee, M.M.K., Effect of plate end and adhesive spew geometries on stresses in retrofitted beams bonded with a CFRP plate, *Compos: Part B*, 39 (2008) 731-739.
- [5] Kim, T.H., Kweon, J.H., Choi, J.H., An experimental study on the effect of overlap length on the failure of composite-to-aluminum single-lap bonded joints, *J. Reinf. Plast. Compos.* 27 (2008) 1071-1081.
- [6] Volkersen, O., Die nietkrafteerteilung in zubeanspruchten nietverbindungen konstanten loschonquerschnitten, *Luftfahrtforschung*, 15 (1938) 41-47.
- [7] Chai, H., Shear fracture, *Int. J. Fract.*, 37 (1988) 137-159.
- [8] Campilho, R.D.S.G., de Moura, M.F.S.F., Barreto, A.M.J.P., Morais, J.J.L., Domingues, J.J.M.S., Fracture behaviour of damaged wood beams repaired with an adhesively-bonded composite patch, *Compos. Part A* 40 (2009) 852-859.
- [9] Campilho, R.D.S.G., de Moura, M.F.S.F., Ramantani, D.A., Morais, J.J.L., Domingues, J.J.M.S., Buckling behaviour of carbon-epoxy adhesively-bonded scarf repairs, *J. Adhes. Sci. Technol.*, 23 (2009) 1493-1513.
- [10] Yoshihara, H., Simple estimation of critical stress intensity factors of wood by tests with double cantilever beam and three-point end-notched flexure, *Holzforschung*, 61 (2007) 182-189.
- [11] Suo, Z., Bao, G., Fan, B., Delamination R-curve phenomena due to damage, *J. Mech. Phys. Solids*, 40 (1992) 1-16.
- [12] Campilho, R.D.S.G., de Moura, M.F.S.F., Pinto, A.M.G., Morais, J.J.L., Domingues, J.J.M.S., Modelling the tensile fracture behaviour of CFRP scarf repairs. *Compos: Part B*, 40 (2009) 149-157.
- [13] Carlberger, T., Stigh, U., Influence of layer thickness on cohesive properties of an epoxy-based adhesive-an experimental study, *J. Adhesion*, 86 (2010) 814-833.
- [14] Ji, G., Ouyang, Z., Li, G., Ibekwe, S., Pang, S.S., Effects of adhesive thickness on global and local mode-I interfacial fracture of bonded joints, *Int. J. Solids Struct.*, 47 (2010) 2445-2458.
- [15] Wambua, P., Ivens, J., Verpoest, I., Natural fibres: can they replace glass in fibre reinforced plastics?, *Compos. Sci. Technol.*, 63 (2003) 1259-1264.
- [16] Ku, H., Wang, H., Pattarachaiyakoop, N., Trada, M., A review on the tensile properties of natural fiber reinforced polymer composites, *Compos.: Part B*, 42 (2011) 856-873.
- [17] Herrera-Franco, P.J., Valadez-González, A., A study of the mechanical properties of short natural-fiber reinforced composites, *Compos: Part B*, 36 (2005) 597-608.
- [18] Campilho, R.D.S.G., Banea, M.D., Pinto, A.M.G., da Silva, L.F.M., de Jesus, A.M.P., Strength prediction of single- and double-lap joints by standard and extended finite element modelling, *Int. J. Adhes. Adhes.*, 31 (2011) 363-372.



- [19] Neto, J.A.B.P., Campilho, R.D.S.G., da Silva, L.F.M., Parametric study of adhesive joints with composites, *Int. J. Adhes. Adhes.*, 37 (2012) 96-101.
- [20] ISO 527-2 standard, *Plastics – Determination of tensile properties – Part 2: Test conditions for moulding and extrusion plastics* (2012).
- [21] Stigh, U., Alfredsson, K.S., Andersson, T., Biel, A., Carlberger, T., Salomonsson, K., Some aspects of cohesive models and modelling with special application to strength of adhesive layers, *Int. J. Fatigue*, 165 (2010) 149-162.
- [22] Rice, J.R., A path independent integral and the approximate analysis of strain concentration by notches and cracks, *J. Appl. Mech.*, 35 (1968) 379-386.
- [23] Banea, M.D., da Silva, L.F.M., Campilho, R.D.S.G., Temperature dependence of the fracture toughness of adhesively bonded joints, *J. Adh. Sci. Technol.* 24 (2010) 2011-2026.
- [24] Campilho, R.D.S.G., Moura, D.C., Gonçalves, D.J.S., da Silva, J.F.M.G., Banea, M.D., da Silva, L.F.M., Fracture toughness determination of adhesive and co-cured joints in natural fibre composites, *Compos: Part B*, 50 (2013) 120-126.
- [25] Bell, A.J., Kinloch, A.J., The effect of the substrate material on the value of the adhesive fracture energy, G_c , *J. Mater. Sci. Lett.*, 16 (1997) 1450-1453.
- [26] Blackman, B.R.K., Kinloch, A.J., Paraschi, M., The effect of the substrate material on the value of the adhesive fracture energy, G_c : Further considerations, *J. Mater. Sci. Lett.*, 20 (2001) 265-267.
- [27] Azari, S., Ameli, A., Datla, N.V., Papini, M., Spelt, J.K., Effect of substrate modulus on the fatigue behaviour of adhesively bonded joints, *Mater. Sci. Eng. A*, 534 (2012) 594-602.
- [28] Mangalgi, P.D., Johnson, W.S., Everett Jr., R.A., Effect of adherend thickness and mixed mode loading on debond growth in adhesively bonded composite joints, *J. Adhesion*, 23 (1987) 263-288.
- [29] Azari, S., Ameli, A., Papini, M., Spelt, J.K., Adherend thickness influence on fatigue behaviour and fatigue failure prediction of adhesively bonded joints, *Compos: Part A*, 48 (2013) 181-191.
- [30] Yan, C., Mai, Y.W., Ye, L., Effect of bond thickness on fracture behaviour in adhesive joints, *J. Adhesion*, 75 (2001) 27-44.
- [31] Khoo, T.T., Kim, H., Effect of bondline thickness on mixed-mode fracture of adhesively bonded joints, *J. Adhesion*, 87 (2011) 989-1019.
- [32] Marzi, S., Biel, A., Stigh, U., On experimental methods to investigate the effect of layer thickness on the fracture behavior of adhesively bonded joints, *Int. J. Adhes. Adhes.* 31 (2011) 840-850.
- [33] Banea, M.D., da Silva, L.F.M., Campilho, R.D.S.G., The effect of adhesive thickness on the mechanical behavior of a structural polyurethane adhesive, *The Journal of Adhesion*, in press.